Temperature induced complementary switching in titanium oxide resistive random access memory

Cite as: AIP Advances **6**, 075314 (2016); https://doi.org/10.1063/1.4959799
Submitted: 23 June 2016 . Accepted: 12 July 2016 . Published Online: 20 July 2016

D. Panda, F. M. Simanjuntak, and T.-Y. Tseng

Temperature induced complementary switching in titanium oxide resistive random access memory

D. Panda,[1,2,a] F. M. Simanjuntak,[2] and T.-Y. Tseng[2]
[1]*Department of Electronics Engineering, National Institute of Science and Technology, Berhampur, Odisha 761008, India*
[2]*Department of Electronics Engineering and Institute of Electronics, National Chiao Tung University, Hsinchu 30010, Taiwan*

(Received 23 June 2016; accepted 12 July 2016; published online 20 July 2016)

On the way towards high memory density and computer performance, a considerable development in energy efficiency represents the foremost aspiration in future information technology. Complementary resistive switch consists of two antiserial resistive switching memory (RRAM) elements and allows for the construction of large passive crossbar arrays by solving the sneak path problem in combination with a drastic reduction of the power consumption. Here we present a titanium oxide based complementary RRAM (CRRAM) device with Pt top and TiN bottom electrode. A subsequent post metal annealing at 400°C induces CRRAM. Forming voltage of 4.3 V is required for this device to initiate switching process. The same device also exhibiting bipolar switching at lower compliance current, Ic <50 μA. The CRRAM device have high reliabilities. Formation of intermediate titanium oxi-nitride layer is confirmed from the cross-sectional HRTEM analysis. The origin of complementary switching mechanism have been discussed with AES, HRTEM analysis and schematic diagram. This paper provides valuable data along with analysis on the origin of CRRAM for the application in nanoscale devices. [http://dx.doi.org/10.1063/1.4959799]

INTRODUCTION

Feature size (F) of the nonvolatile memory is scaling down toward nanometer size, because of the drive toward faster, smaller, and denser nano-electronics systems. As one continues to shrink cell size, it becomes ever more complicated to sustain a sufficient number of electrons in these charge storage based memories. Among the several emerging memory, resistive random access memory (RRAM) based on the resistive switching (RS) effect taking place in metal-insulator-metal (MIM) cells, has attracted renowned interests as a promising next generation nonvolatile memory owing to its simple constituents, high speed operation, nondestructive readout, low operation voltage, long retention time, and high scalability.[1–7] Binary transition metal oxides, such as SiO_2, HfO_2, TiO_2, NiO, ZnO, Ta_2O_5, etc.,[1–18] has been intensively investigated as an active layers in RRAM application, for their big advantage, like crystal structure and stoichiometry are more easily controlled than perovskite oxides that consist of more than three components.

Two-terminal RRAM structure allow its integration in crossbar arrays, by accessing each memory cell through the selection of a word-line and a bit-line.[1,4] Small device size of $4F^2$ and the availability of 3-D architecture solutions in a crossbar array,[10] make RRAM a promising competitor of flash NAND device. On the contrary, select device, used to avert the sneak-path current of unselected cells in low resistance state (LRS), is one of the main challenge for getting high-density RRAM crossbar arrays.[4,11] To resolve this concern, several approaches like, threshold switches,[12]

[a]Corresponding author: dpanda@nist.edu

oxide diodes,[4] and self-rectifying RRAM[13] have been proposed. Recently, complementary resistive switch was attracted renewed interest for coding the logic bit in two different reset (high resistance) states to resolve the sneak-path issue, without using any select devices.[14,15] Recent report[19] suggest that complementary resistive switching can be achieved by fabricating back-to-back RRAM cells configuration, however, the approach requires complicated process flow and time consuming.

In this work, we report annealing induced complementary switching (CS) in TiN/TiO_xN_y/TiO_2/Pt (TTTP) structure having TiN as a bottom electrode. Complementary switching performances and mechanism in the TTTP structures are associated with the charged oxygen vacancies. At nanoscale, the forming voltage (V_f) and the switching characteristics significantly controlled by the quantity of oxygen vacancies. The physical and resistive switching properties of TiN/TiO_xN_y/TiO_{2-x}/Pt structures are investigated. Using analytical ion-migration models the complementary switching mechanism is finally discussed.

RESULTS AND DISCUSSION

A 17 nm thin TiO_2 thin film was grown by rf magnetron sputtering on Si/SiO_2/Ti/TiN substrate. A Pt (20 nm) top electrodes (diameter: 150 μm) were deposited by e-beam evaporation to form Si/SiO_2/Ti/TiN/TiO_2/Pt structure for memory device characterization. Subsequently, the devices were annealed (PMA) at 400°C to 550°C for 1-2 min in oxygen ambient for oxidation. Control sample with TiO_2 (as-deposited) having same thickness is also prepared under the same condition for comparison. To probe the thickness of the layers, cross-sectional high resolution transmission electron microscopic (HRTEM) observations were performed using JEOL JEM-2010F. Auger electron spectroscopy (AES) (VG Scientific Microlab 310F) is used to study the composition of the stacked structures at different depth. Electrical complementary switching characteristics at the TTTP structure are measured using Agilent B1500A analyzer. Voltage bias is applied on the Pt top electrode, whereas TiN bottom electrode is grounded during electrical measurement.

A forming process (measured at 0 to +6 V, I_{cc} =1 mA) is necessary to activate the initial device, a positive forming voltage (V_f) of ~4.3 V is essential to initiate the complementary switching process. Voltage is applied on the Pt top electrode, whereas TiN bottom electrode is grounded during whole measurement. Figure 1(a) shows the typical forming curve of the TiO_2 based TTTP CRRAM device after annealed at 400°C. The current is abruptly increases from ~690 pA to the set compliance of 1 mA (I_{cc}) during forming process and the device switches from pristine resistance state (PRS) to the low resistance state (LRS). To reset the electroformed device, a negative voltage of -3 V, without any compliance is applied. A reset voltage (V_{Reset}) of ~-1.8V is required to return the device to high resistance state (HRS) again, as shown in the figure 1(a). After the initial (first) reset, the device is able to work at lower current operation. Current compliance of 0.1 μA is applied during set process while no compliance is applied during reset (LRS to HRS) the device. Figure 1(b) shows typical bipolar current voltage (I-V) switching characteristics of a

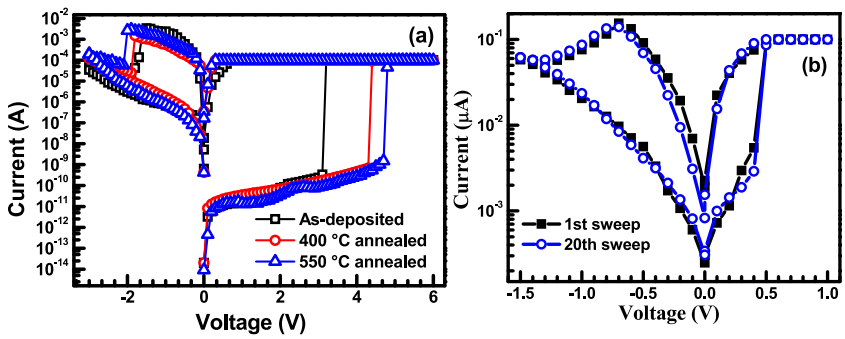

FIG. 1. Typical (a) current-voltage forming characteristics of the as-deposited, 400°C and 550°C annealed and (b) bipolar current-voltage characteristics of the 400°C annealed TiN/TiO_xN_y/TiO_{2-x}/Pt RRAM device in semi-log scale.

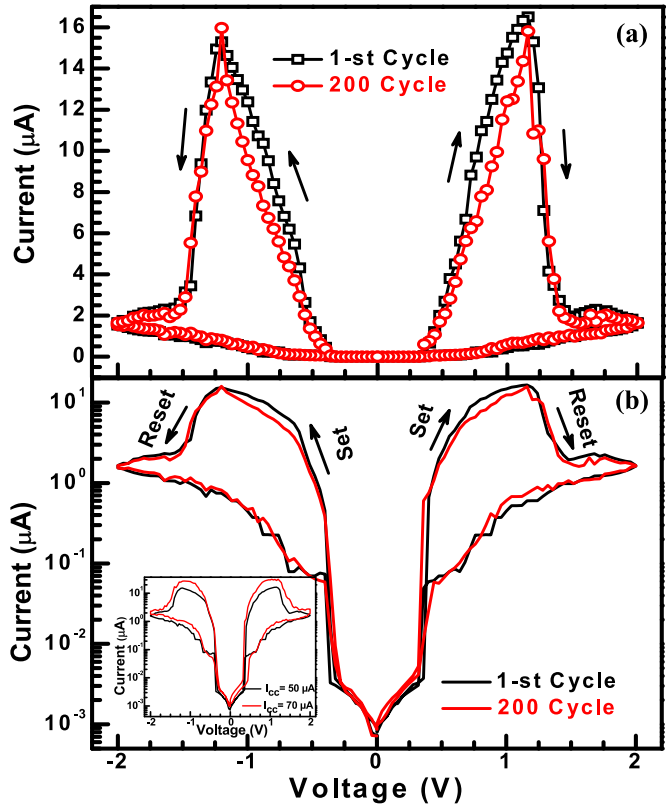

FIG. 2. Complementary current-voltage switching characteristic of the 400°C annealed TiN/TiO_xN_y/TiO_{2-x}/Pt RRAM device (a) linear scale and (b) semi-log scale having 50 μA compliance current. Inset of (b) shows the current-voltage switching characteristic of the same device with compliance current 50 μA and 70 μA.

Si/SiO_2/Ti/TiN/TiO_xN_y/TiO_{2-x}/Pt RRAM structure. A set voltage (V_{set}) of 0.4 V and V_{reset} of −0.7 V are required to set and reset the device, respectively. Such bipolar-switching characteristics as shown in figure 1(b) are typical for TiO_{2-x} based resistive memory devices. As deposited and 550°C annealed devices are also show bipolar switching after forming at 3.1 V and 4.7 V respectively, as shown in figure 1(a).

Interestingly, a complementary switching can be observed along with bipolar switching in the 400°C annealed device only, when the compliance current is increased to 50 μA during voltage sweeping, as shown in figure 2. Almost similar CRRAM characteristics are also detected by setting higher compliance current (>50 μA), as shown in inset of figure 2(b). Due to I_{cc} limitation, most of the available oxygen vacancies do not contribute to migration and remain at the cathode. Here I_{cc} controls the amount of positively charged oxygen vacancies, which are produced for migration from the bottom cathode toward the top anode.[2,3,20] For the RRAM based on binary oxides sandwiched by the inert electrodes, the reversible switching is mainly attributed to oxygen vacancies or oxygen ions. It's well established that transport mechanism of TiO_{2-x} based bipolar RRAM can be well modeled with tunneling barrier or other non-linear transport barrier.[20,21] The electronic conduction of such devices can be modulated by inducing the motion of ionized defects, such as oxygen vacancies, by applying an appropriate voltage across the device.[2,3,22]

Using defect chemistry the filament formation mechanisms of titanium oxides can be explained. TiO_{2-x} is a type of hypostoichiometric transition metal oxides (TMOs).[23] Hypostoichiometry ($MO_{x-\delta}, \delta > 0$) results from the formation of (i) oxygen vacancies or (ii) cation interstitials.[24] The formation reactions for (i) and (ii) of TiO_{2-x} are expressed in the Kröger–Vink notation[25] as

$$O_O^{\times} \rightarrow V_O^{\bullet\bullet} + 2e^- + \frac{1}{2}O_2(g) \quad (1)$$

and

$$Ti_{Ti}^{\times} + O_O^{\times} \rightarrow Ti_i^{\bullet\bullet} + 2e^- + \frac{1}{2}O_2(g) \quad (2)$$

Where, positive charge is represented by a dot (•), and neutral by (×). *V* for a vacancy or *Ti* for a Titanium ion. The subscript represents defect site (*i*) for interstitial, (*Ti*) for Titanium lattice site.

To support this explanation, figure 2 shows the current-voltage (I-V) characteristics of the device by setting I_C =50 μA. A set transition, i.e., HRS to LRS, is observed during positive cycle at ~0.36 V, as shown in figure 2, except the current is increasing to a maximum value of ~15.8 μA at 1.16 V. After set transition, further increase of the positive voltage causes changes of resistance state to high resistance state or reset transition insisted. The complete reset occurred during positive cycle at 1.44 V. Quite similar characteristics is also detected during negative voltage sweeping. A set transition is observed during negative cycle at ~-0.28 V. As the current compliance value set at 50 μA, the current value increased to maximum value 15.96 μA at -1.2 V and current starts decreases or device starts resets for the further increases of negative voltage. During negative cycle the complete reset occurs at -1.52 V. Figure 1(a) shows the linear I-V curve, whereas, figure 2(b) shows the semi-log I-V characteristics. Alternate application of positive and negative sweeps exclusive of current compliance limitations thus permits for programming the RRAM in two unusual reset states.[26] This can serve for encoding two logic bits in passive crossbar arrays, without any requirement of select device.[14,27]

The cycling measurements were repeated by the dc sweep. Endurance of the Pt/TiO_x/ TiO_xN_y/ TiN structure after annealing is presented in figure 3(a) and 3(b) for positive and negative switching cycles, respectively. The current value measured at @ ±1.12 V. Figure 3 reveals that HRS/LRS ratio is higher than 10^2 times, without any noticeable degradation and much fluctuations even after 200 switching cycles. Note that the device performs no data loss after 10^3 seconds (data not shown).

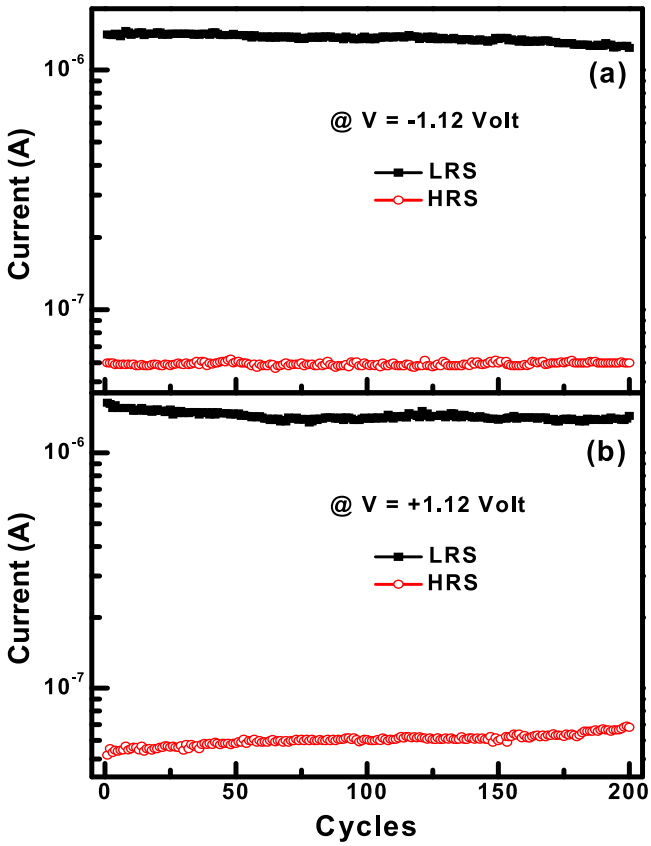

FIG. 3. Endurance characteristics of the CRRAM device (a) negative cycles and (b) positive cycles.

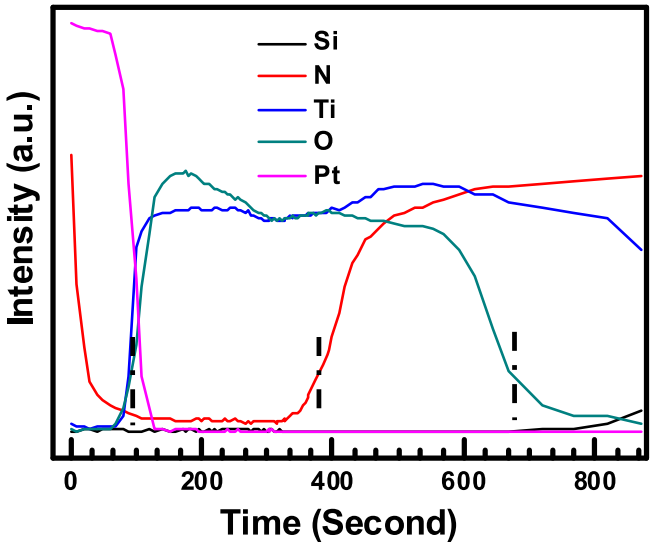

FIG. 4. Typical AES spectra of TiN/TiO_xN_y/TiO_{2-x}/Pt CRRAM device.

In order to study the switching mechanism in details, compositional analysis is necessary of the TTTP structure. Figure 4 shows the typical AES spectra of the annealed CRRAM device. A clear oxygen gradient is observed from the spectra. After annealing, a layer of TiO_xN_y having almost same thickness of TiO_{2-x} (~10 nm) is formed by intermixing between TiO_2 and TiN at the bottom electrode junction. There are no nitrogen atoms inter-diffusion is observed throughout TiO_2 layer after annealing based on the measurement and analysis of the AES spectra, as shown in figure 4. As seen from the figure, the oxygen atom concentration decreases after 300 seconds and it is almost zero after 660 seconds etching, due to the intermixing at the junction by the diffusion of oxygen atoms. It attributes the formation of interfacial TiO_xN_y gradient layer at TiN/TiO_{2-x} interface by the inter-diffusion of oxygen atoms from the TiO_2 layer to the TiN bottom electrode after annealing. This oxygen gradient plays a crucial role during complementary switching mechanism, as discussed in figure 6.

To probe the thickness and confirm the formation of intermediate layer, which is obtained from AES result, cross sectional HRTEM analysis is employed to determine the difference between as-deposited and annealed TTTP structures. The TEM image of a typical as-deposited sample is shown in figure 5(a), clearly shows the 17 nm TiO_2 layer is present between TiN and Pt layers. There are no sign of intermixing at the TiN/TiO_2 interface. Figure 5(b) shows the typical cross sectional HRTEM image of the 400°C annealed film. However after annealing the sample at 400°C, a clear colour contrast gradient is observed in figure 5(b) indicating that a formation of a 10 nm thin interfacial TiO_xN_y layer between TiN and TiO_{2-x} layers. After intermixing the self-assembled layer exists in the film. The thickness of the remaining TiO_{2-x} layer is found to 10 nm. This result corroborates with the results obtained from the AES spectra.

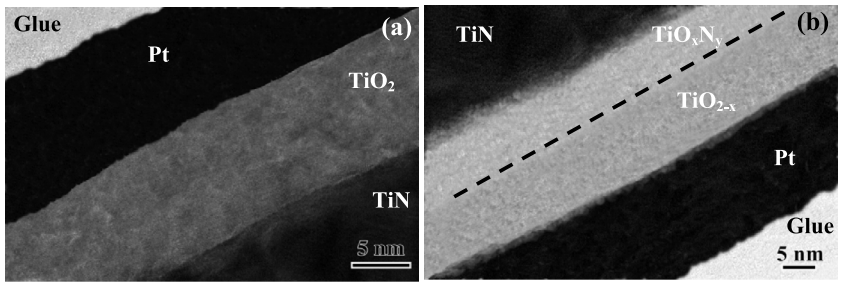

FIG. 5. Cross sectional HRTEM image of the (a) as deposited and (b) 400°C annealed TiN/TiO_2/Pt RRAM structure.

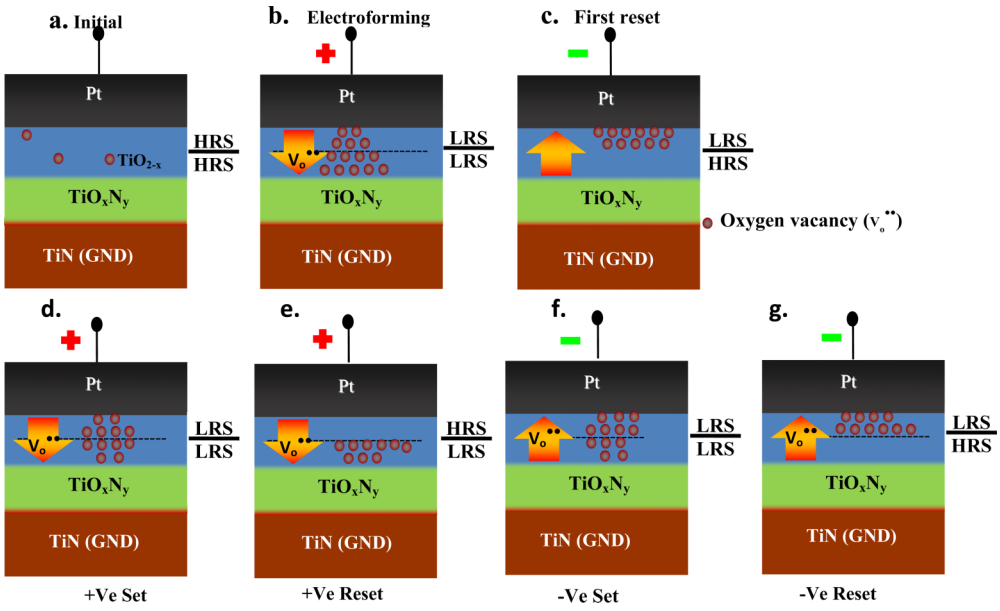

FIG. 6. Schematic complementary switching mechanism of $TiN/TiO_xN_y/TiO_{2-x}/Pt$ device.

The switching mechanism of the binary oxides based RRAM devices can be explained by taking into account the oxygen vacancy migration under a bias voltage and the contributions of both the TiO_{2-x}/TiO_xN_y bottom and Pt/TiO_{2-x} top interfaces.[2,3,26] AES spectra reveals that there is an oxygen gradient inside the film. So, we can assumed that the TiO_{2-x} layer is to consist of two resistor regions in a series: one at the TiO_{2-x}/TiO_xN_y bottom interface (R_{bot}) and another one at the Pt/TiO_{2-x} top interface (R_{top}), as marked in figure 6(a). The changes of resistances in these two layer leads to complementary switching. However, the bottom interfacial TiO_xN_y layer is always believed to be in LRS and acts as an oxygen reservoir, which modulates the oxygen vacancy concentration to control the complementary switching in the bottom TiO_{2-x}/TiO_xN_y interface. The initial state of the memory cell is in HRS, when both the R_{top} and R_{bot} interfaces are in HRS (R_{top}/R_{bot} in HRS/HRS), as shown in figure 6(a).

During forming process positive bias voltage is applied on top electrode, a huge amount of oxygen vacancies are introduced in the TiO_{2-x} layer towards bottom electrode. This oxygen vacancies leads to formation of an oxygen deficient conductive channel or filament and allows the device to be switched to LRS (R_{top}/R_{bot} in LRS/LRS), as shown in figure 6(b). As mentioned in equation (1), oxygen gas evolution problem can be solved by explaining the evolution of oxygen vacancy formation from the oxygen atom, which is stored at the TiO_xN_y oxygen reservoir layer, through an oxidation or/ and a physical adsorption process. To reset the device after forming a negative voltage of -1.5 V is applied at the top electrode, which attracts positively charged oxygen vacancies and a large amount of oxygen vacancies drifted from the bottom interface region to top interface region. As a result, the filament at the lower region of the TiO_{2-x} i.e., closed to the TiO_{2-x}/TiO_xN_y interface layer, will be ruptured and resistance state changed to HRS. But, the filament at the upper region remains unaffected or still in LRS, as shown in figure 6(c). Since, once one side filament is ruptured there are no flow of electrons.

As mentioned before, complementary switching is observed after increasing the compliance current to 50 μA. Once we applied positive voltage with 50 μA compliance current, the positively charged oxygen vacancies are start to forming filament from the Pt/TiO_{2-x} top interface. At a positive voltage of 0.36 V (i.e., V_{Set}) the filament at bottom interface is completely formed and both the regions are changed to LRS, as shown in figure 6(d). Further increase of positive voltage ($V > V_{Set}$) the charged oxygen vacancies are depleted at the top interface, leads to change to HRS by rupturing the filament at Pt/TiO_{2-x} top interface, as shown in figure 6(e).

In the case of negative applied voltage with higher compliance current (50 μA), the oxygen vacancies are attracted towards Pt top electrode and by drift motion the filament is start to form. At set

voltage of -0.28 V, the complete filament is formed at the two regions in the TiO_{2-x} layer and both the regions are changed to LRS and device is set state now, as shown in figure 6(f). Further increase of negative voltage the oxygen vacancies are start to deplete from the bottom TiO_{2-x}/TiO_xN_y interface and the filament is ruptured, states changed to HRS, as shown in figure 6(g). Which leads to reset the device. From the above mechanism it's cleared that the complementary switching depends on the amount of oxygen vacancies present inside the TiO_{2-x} layer for this structure. It is also important that an appropriate amount of power is required to make movable the oxygen vacancies. Since, at lower compliance current the same device acts as a bipolar switch, due to the insufficient power to make movable oxygen vacancies. So, not only appropriate amount of oxygen vacancies, the amount of power is also an important parameter to achieve the complementary switching.

CONCLUSION

In summary, a novel approach to transition from bipolar switching to complementary switching of a $TiN(BE)/TiO_xN_y/TiO_{2-x}/Pt(TE)$ structure has been demonstrated. A forming process is essential for the all as-deposited and annealed devices to initiate the forming process. All the devices shows bipolar switching below 50 μA compliance current. The 400°C annealed device acts as a complementary switch above 50 μA compliance current. During CRRAM operation the device set at 0.36 V and reset at 1.44 V during positive cycle and for negative cycle set at -0.28 V and reset at -1.2 V. The CRRAM device shows good endurance and retention. A clear formation of oxygen gradient layer at TiO_{2-x} and interfacial 10 nm TiO_xN_y layer are observed from AES and HRTEM spectra. Based on AES and HRTEM observation and with the help of schematic structures the complementary switching mechanism is explained. This structure has the potential for use in highly dense crosspoint memory without the cell selection devices.

[1] I.G. Baek, D.C. Kim, M.J. Lee, H.-J. Kim, E.K. Yim, M.S. Lee, J.E. Lee, S.E. Ahn, S. Seo, J.H. Lee, J.C. Park, Y.K. Cha, S.O. Park, H.S. Kim, I.K. Yoo, U. Chung, J.T. Moon, and B.I. Ryu, *IEEE Int. Devices Meet. 2005. IEDM Tech. Dig.* (IEEE, 2005), pp. 750–753.
[2] D. Panda and T.-Y. Tseng, Thin Solid Films **531**, 1 (2013).
[3] D. Panda and T.-Y. Tseng, Ferroelectrics **471**, 23 (2014).
[4] M.J. Lee, Y. Park, B.S. Kang, S.E. Ahn, C. Lee, K. Kim, W. Xianyu, G. Stefanovich, J.H. Lee, S.J. Chung, Y.H. Kim, C.S. Lee, J.B. Park, I.G. Baek, and I.K. Yoo, Tech. Dig. - Int. Electron Devices Meet. IEDM 771 (2007).
[5] F.M. Simanjuntak, D. Panda, T.-L. Tsai, C.-A. Lin, K.-H. Wei, and T.-Y. Tseng, Appl. Phys. Lett. **107**, 033505 (2015).
[6] D. Panda and T.-Y. Tseng, J. Mater. Sci. **48**, 6849 (2013).
[7] D. Panda, C.Y. Huang, and T.Y. Tseng, Appl. Phys. Lett. **100**, 112901 (2012).
[8] F.M. Simanjuntak, O.K. Prasad, D. Panda, C.-A. Lin, T.-L. Tsai, K.-H. Wei, and T.-Y. Tseng, Appl. Phys. Lett. **108**, 183506 (2016).
[9] F.M. Simanjuntak, D. Panda, T.-L. Tsai, C.-A. Lin, K.-H. Wei, and T.-Y. Tseng, J. Mater. Sci. **50**, 6961 (2015).
[10] H.S. Yoon, I.-G. Baek, J. Zhao, H. Sim, M.Y. Park, H. Lee, G.-H. Oh, J.C. Shin, I.-S. Yeo, and U.-I. Chung, 2009 Symp. VLSI Technol. 26 (2009).
[11] J. Liang and H.S.P. Wong, IEEE Trans. Electron Devices **57**, 2531 (2010).
[12] M.-J. Lee, Y. Park, D.-S. Suh, E.-H. Lee, S. Seo, D.-C. Kim, R. Jung, B.-S. Kang, S.-E. Ahn, C.B. Lee, D.H. Seo, Y.-K. Cha, I.-K. Yoo, J.-S. Kim, and B.H. Park, Adv. Mater. **19**, 3919 (2007).
[13] X.A. Tran, W.G. Zhu, B. Gao, J.F. Kang, W.J. Liu, Z. Fang, Z.R. Wang, Y.C. Yeo, B.Y. Nguyen, M.F. Li, and H.Y. Yu, IEEE Electron Device Lett. **33**, 585 (2012).
[14] E. Linn, R. Rosezin, C. Kügeler, and R. Waser, Nat. Mater. **9**, 403 (2010).
[15] J. Lee, J. Shin, D. Lee, W. Lee, S. Jung, M. Jo, J. Park, K.P. Biju, S. Kim, S. Park, and H. Hwang, Tech. Dig. - Int. Electron Devices Meet. IEDM 452 (2010).
[16] D. Panda, A. Dhar, and S.K. Ray, J. Appl. Phys **108**, 104513 (2010).
[17] D. Panda, A. Dhar, and S.K. Ray, IEEE Trans. Nanotechnology **11**(1), 51 (2012).
[18] D. Panda and M. Panda, J. Nanoscience and Nanotechnology **16**(1), 1216 (2016).
[19] S.-M. Lin, J.-S. Huang, W.-C. Chang, T.-C. Hou, H.-W. Huang, C.-H. Huang, S.-J. Lin, and Y.-L. Chueh, ACS Appl. Mater. Interfaces **5**, 7831 (2013).
[20] J.J. Yang, M.D. Pickett, X. Li, D. a a Ohlberg, D.R. Stewart, and R.S. Williams, Nat. Nanotechnol. **3**, 429 (2008).
[21] R. Waser, D. Jeong, and H. Schroeder, Phys. Rev. B **79**, 195317 (2009).
[22] M.D. Pickett, D.B. Strukov, J.L. Borghetti, J.J. Yang, G.S. Snider, D.R. Stewart, and R.S. Williams, J. Appl. Phys. **106** (2009).
[23] L. Eyring and M. O'Keeffe, Acta Crystallogr. Sect. B Struct. Crystallogr. Cryst. Chem. **27**, 1839 (1971).
[24] M.W. Barsoum, *Fundamentals of Ceramics* (Taylor and Francis, New York), Vasa 622 (2003).
[25] F.A. Kröger and H.J. Vink, *Solid State Phys. - Adv. Res. Appl.* (1956), pp. 307–435.
[26] D. Panda, A. Dhar, and S.K. Ray, RSC Adv. **5**, 33283 (2015).
[27] F. Nardi, S. Balatti, S. Larentis, and D. Ielmini, *Tech. Dig. - Int. Electron Devices Meet. IEDM* (2011).